DEVELOPMENT OF A LOW ENERGY NEUTRON SOURCE FOR BUBBLE CHAMBER CALIBRATIONS

Salvatore Zerbo
Advisor: Russell Neilson

Submitted in partial fulfillment of the requirements for the degree of Bachelor of Science in Physics

Drexel University
Philadelphia, PA
June 2019

Contents

Abstract

The use of bubble chambers for direct dark matter detection requires high sensitivity to energy levels in the range of 1-100 keV and strict measures to reduce background radiation. Neutrons can be used to simulate WIMP elastic scattering interactions with the target volume in order to ensure high detection efficiency. We aim to develop a low energy neutron source that will allow us to properly calibrate bubble chambers to ensure their ability to detect such events. We propose a solution consisting of a neutron source composed of a radioisotope capable of emitting gamma radiation at the required energy thresholds and a target capable of ejecting photoneutrons when struck by the gamma radiation. We have chosen seven main candidates for a gamma source, taking note of important properties such as half-life, availability, cost, and many others. We have also calculated the theoretical energies of the neutrons emitted by each source and the rate at which each source would emit neutrons. We utilize the GEANT4 simulation software to explore various scenarios and determine effective neutron emission rates and the energies upon interaction with the C_3F_8. Results yielded from the Drexel Bubble Chamber will be useful for other members of the PICO collaboration and other direct detection experiments.

1 Introduction

1.1 Dark Matter & Bubble Chambers

The nature of cosmological dark matter has been an elusive mystery for many decades despite occupying nearly a quarter of the universe's content[1]. The modern theory of Weakly Interacting Massive Particles (WIMPs) requires highly specialized detection methods. WIMPs as the leading candidate address many critical issues in the ΛCDM Model such as galaxy rotation curves, the gravitational lensing of light in underdense regions, and the flatness of the universe[2].

Bubble chambers have been used since the early 1950's as particle detectors[3] and have more recently been adapted for the detection of WIMPs. Bubble chambers function by

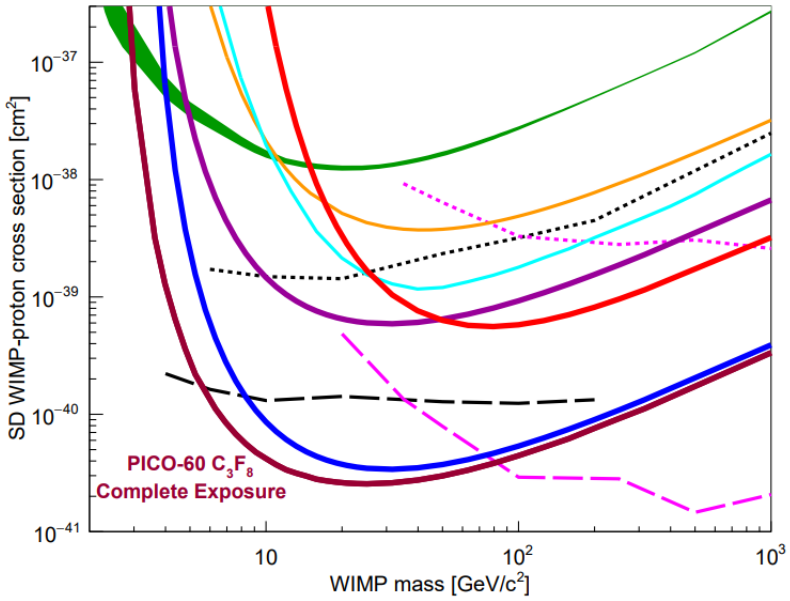

Figure 1: Latest spin dependent constraints on the WIMP-nucleon cross section from PICO-60[6]. Other relevant results include the first blind exposure of PICO-60 C3F8 (thick blue), as well as limits from PICO-60 CF3I (thick red), PICO-2L (thick purple), and PICASSO (green band).

maintaining a liquid in a superheated state through tuning its temperature and pressure. Once in this state, any particle that deposits energy greater than the threshold energy will result in bubble nucleation. The PICO Collaboration uses the concept of bubble chambers with superheated fluorine-based liquids to provide some of the strongest constraints on the WIMP nucleon cross-sections as illustrated in Figure 1[4].

The ability to achieve low background is critical to direct detection methods of WIMPs. Several design decisions have been included to maximize detection efficiency and ensure accuracy of events. Fluorine based liquids are especially appealing as a target volume due to their insensitivity to gamma and beta particles[5]. The use of piezoelectric sensors allows for discrimination of alphas by acoustic analysis. Muons are eliminated through the use of a water tank containing PMT's. Reconstruction of events in the target volume allows for discrimination of neutron events due to bubble multiplicity.

Previous bubble chambers[6] in the PICO collaboration utilized an up-side down design where the target volume was placed below a buffer fluid as seen in Figure 2a. This chamber

faced many issues in the form of particulate falling down into the target volume and other issues at the water-target fluid interface. The Drexel Bubble Chamber is a prototype right-side up design that aims to remove these issues by flipping the design. In order to isolate the target volume, we use a sharp temperature gradient between the active and non-active regions of the chamber as seen in Figure 2b.

The bubble chambers require calibrations with several types of sources to ensure that each particle is detected and identified correctly. Most importantly, we must be sure that the conditions of the chamber allow for detection of WIMPs. As result, the detector must be sensitive to elastic scattering interactions from nuclear recoils in energy ranges of 1-100 keV. The best method for determining the efficiency of nuclear recoils is through low energy neutron calibrations.

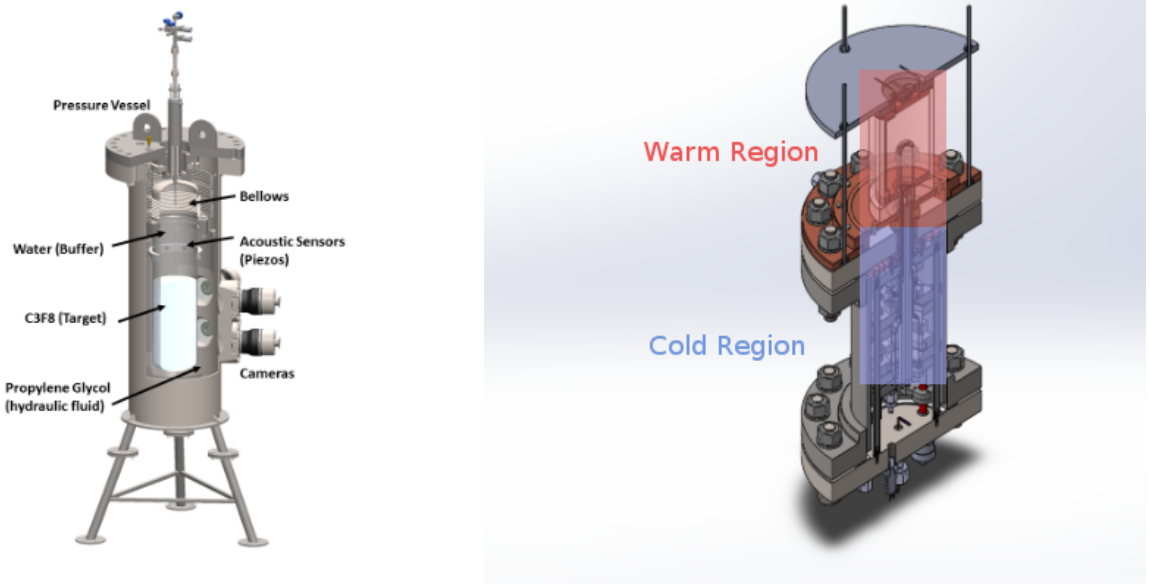

(a) (b)

Figure 2: (a) Design of PICO-60 bubble chamber. This design places the target volume below a water buffer layer. (b) CAD design of the right-side up Drexel Bubble Chamber.

1.2 Low Energy Neutrons

Neutrons can be generated through many different methods such as spontaneous fission, α interactions on a low-atomic-weight target, γ interactions with a target such as ^{9}Be or ^{2}D, or through neutron generators. We desire to generate neutrons at relatively low ($\leq$ 200 keV) energy scales, and as a result, the only viable method for a neutron source is through γ interactions upon a target. Although the other methods may satisfy many of the requirements, they are only capable of producing neutrons on the MeV energy scale, which is a vital component to this project. We require low energy neutrons to properly calibrate bubble chambers for WIMP events which will occur at similar energy levels. Without neutron calibration, it is impossible to tell if the chambers are able to efficiently and accurately detect potential WIMP events.

Neutron sources for chamber calibrations have been considered before within the PICO collaboration[7]–[9]; however, a low energy neutron source has yet to be developed. The components of our neutron source will include a gamma source, target material, and appropriate shielding to prevent gammas and neutrons from leaking in undesired directions. Starting with an isotope that undergoes some form of decay, it will then emit gammas at a monoenergetic level. If the gamma contains more energy than the threshold for neutron production, it will deposit enough energy upon contact and emit a neutron. The neutron will then come into contact with the bubble chamber and deposit its energy on to superheated C_3F_8. From there, our chamber will detect an event trigger, and we will be able to perform calibrations through image analysis, piezoelectric acoustic data, and other simulations.

$$\begin{aligned} {}^{9}Be + \gamma &\longrightarrow {}^{8}Be + n \\ {}^{2}D + \gamma &\longrightarrow {}^{1}D + n \end{aligned} \tag{1}$$

Equation 1 shows the reactions of the targets with an incident gamma and the resulting isotopes and particles. From this equation, we are able to determine the threshold energy

of the gammas needed to emit one neutron from each nucleus with simple conservation of energy. Since the number of electrons does not change during this process, we are free to emit them from the calculations since they will cancel. A similar calculation for ^2D is omitted, but yields 2.23 MeV. For the ^9Be target, we have

$$\begin{aligned} m_{^9Be} * c^2 + Q &= m_{^8Be} * c^2 + m_n * c^2 \\ \Rightarrow Q &= (m_{^8Be} + m_n - m_{^9Be}) * c^2 = 1.67\ MeV \end{aligned} \tag{2}$$

The key difficulty in designing a low energy neutron source is finding an isotope that fits all of our requirements. The isotope must have a long enough half-life such that it can survive through the extensive safety procedures at Snolab without losing a majority of the material. It should also produce gammas close to the threshold energy of the target such that the emitted neutron will be in our desired energy range. It is important to have large branching ratios for these gamma energies so that we obtain neutrons primarily at the energy we desire. Finally, the isotope should be feasible to buy in large enough quantities without either costing too much or requiring too much time to be delivered.

2 Methods

2.1 Identifying the Proper Gamma Source

Our first approach to tackling this problem is to create an exhaustive list of all potential candidates for gamma sources and note the specific properties that we require them to have. Included in the list will be each candidates gamma energy spectrum, branching ratios, half-life, and other information on the feasibility of acquiring the isotope. Another important property to keep track of is the neutron production rate. If the rate is too low, then we will not be able to perform accurate calibrations; however, we also want to avoid too many neutrons from being produced, as this could cause unwanted leakage that could cause issues elsewhere.

Isotope	Target	Half-Life (Years)	Main Gamma Energy (keV)	Branching Ratios (%)
^{26}Al	^{9}Be	7.17E+05	1808	99.76
^{207}Bi	^{9}Be	31.55	1770	6.87
^{58}Co	^{9}Be	0.19	1674	0.52
^{150}Eu	^{9}Be	36.9	1690	0.15
^{124}Sb	^{9}Be	0.16	1690	47.79
^{88}Y	^{9}Be	0.29	1836	99.2
^{226}Ra(^{214}Bi)	^{2}D	1590	2447	1.57

Table 1: List of potential gamma radioisotope sources with their corresponding targets, half-lives, relevant gamma energies, and branching ratios gathered from the Table of Isotopes.

By searching the Table of Isotopes, a list has been developed as seen above in Table 1. The seven isotopes listed are the most likely in terms of their branching ratios, gamma energies, half-lives, and feasibility of being obtained. Most gamma sources do not emit >2 MeV, so finding a source to use with a ^{2}D target is unlikely outside of ^{226}Ra.

2.2 Calculations

After gathering the list of potential gamma sources, our next step is to calculate and gather as much information about each of the isotopes to better inform our decision. This data is listed below in Table 2. The expected theoretical neutron energies for each system is calculated through[10]:

$$E_n = \frac{A-1}{A}[E_\gamma - Q - \frac{E_\gamma^2}{1862(A-1)}] + \delta; \tag{3}$$

Here, A is the mass number, E_γ is the energy of the incident gamma, Q is the threshold energy for the target, and δ is an energy spread function defined by:

$$\begin{aligned} \delta &\approx E_\gamma[\frac{2(A-1)(E_\gamma - Q)}{931A^3}]^{1/2} cos(\theta) \\ \delta_{max} &= 2E_\gamma[\frac{2(A-1)(E_\gamma - Q)}{931A^3}]^{1/2} \end{aligned} \tag{4}$$

The angle θ is defined as the angle between the incident gamma and the emitted neutron.

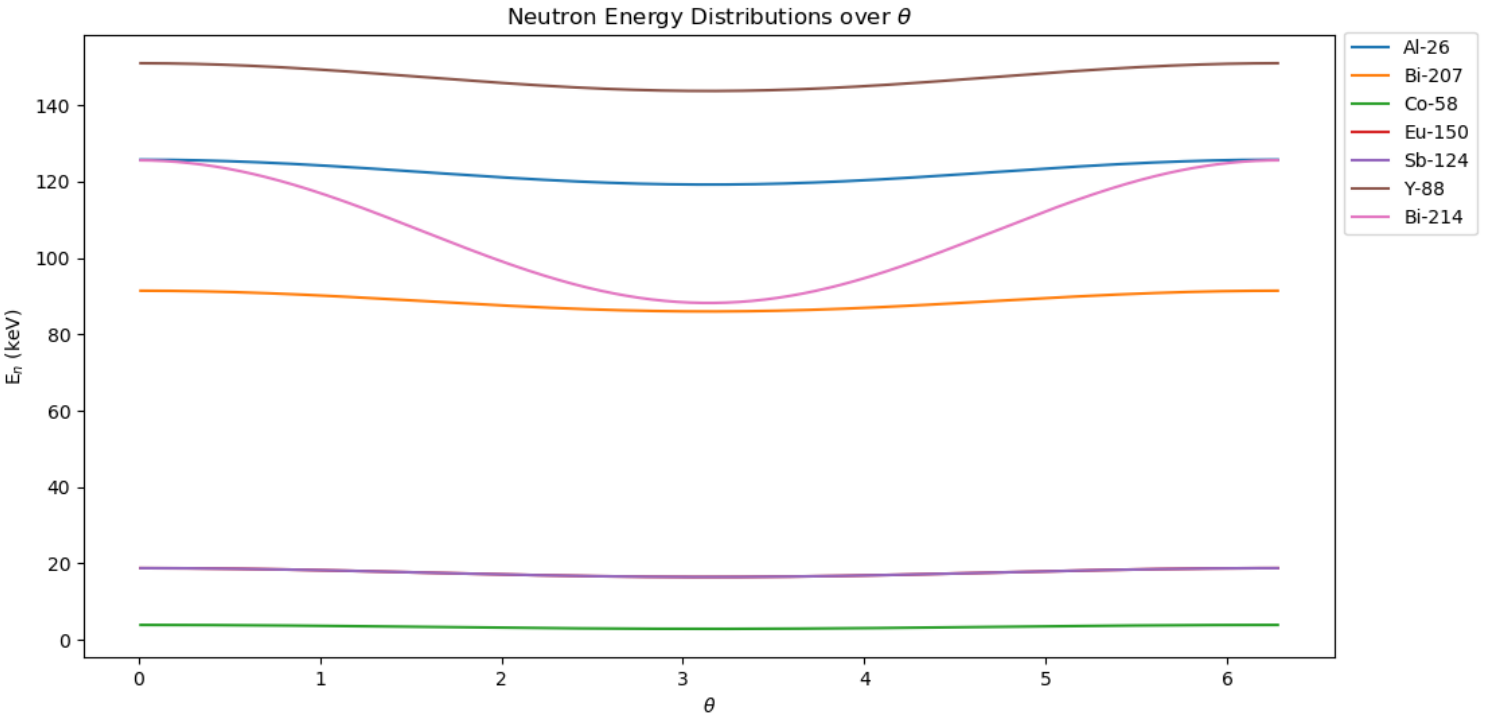

Figure 3: Expected neutron energies over a range of incident gamma angles from 0 to 2π. This is shown for each of our potential sources. Some like ^{214}Bi have large variability while most only vary by a few keV.

As seen in Figure 3, the θ dependence of δ can have significant effects, and it is difficult to determine the value of θ, so we will place the gamma source such that the gammas are incident in an isotropic manner, yielding δ_{max} instead.

Next, we estimate the rate at which neutrons will be emitted from each system. We first start with basic assumptions that will allow for convenience when doing the calculations: we will have 1g of material for both the gamma source and target, and the distance between the source and target will be 1cm. From the half-life of the gamma source, the decay constant, and subsequently, the activity can be calculated:

$$t_{1/2} = \frac{ln(2)}{\lambda} \implies \lambda = \frac{ln(2)}{t_{1/2}}$$

$$A = \lambda N$$

Isotope	Theoretical Neutron Energy (keV)	n/s/g
^{26}Al	128.99	539
^{207}Bi	94.14	1.52E+05
^{58}Co	4.42	2.27E+07
^{150}Eu	19.93	2.51E+04
^{124}Sb	19.93	2.07E+09
^{88}Y	154.62	3.34E+08
^{226}Ra(^{214}Bi)	144.25	9.00E+03

Table 2: Gamma sources with their corresponding expected neutron energies and neutron rates.

Then the number of neutrons can be estimated through the most relevant factors: activity, branching ratio, the amount of target, the gamma-neutron cross section, and the spherical surface area covered by the isotropic emission of gammas. The gamma-neutron cross section can be found by reading them off plots from JANIS for each specific incident gamma energy. Combining these factors leads to equation 5:

$$\#n \approx A * \%Branching * \frac{m_{target}}{m_{target\ nucleus}} * \sigma * \frac{1}{SA_{sphere}} \tag{5}$$

Two more calculations were done to determine how much deuterium is found per amount of heavy water, since that is the most available form, and how large would a sphere of that amount of heavy water be. The first is simply calculated by taking the ratios of the masses, so if we desire 1g of Deuterium as was used for the calculations above, we would need 10g of heavy water. The size of a sphere would then be found by equating the mass to the density times the volume of a sphere. This yields a radius of 1.29 cm, which is on the scale of the size that we would like the system to be at.

2.3 Choosing a Source

The availability of our seven potential sources has been determined based on the strength, price, lead time, and supplier. The first isotope to be explored is ^{26}Al, which looks to be

a strong candidate at first; however, it is incredibly difficult and expensive to obtain. Only one supplier, Oak Ridge National Laboratory, is able to provide it at a cost of $381 per nCi. This is incredibly expensive considering we require amounts on the scale of mCi for a neutron rate large enough. ^{150}Eu is extremely is rare, making it infeasible to use for a gamma source. Similarly, ^{58}Co is also expensive and rare, requiring too long of a lead time to acquire.

Of the remaining sources, ^{226}Ra is the weakest due to the available strength of the source and high theoretical neutron energy. This leaves the two most popular gamma sources, ^{88}Y and ^{124}Sb, and ^{207}Bi. Looking at Table 1, it's clear that ^{124}Sb will never make it through the Snolab safety procedures and would be replaced far too often, resulting in high expenses. ^{88}Y, although a strong contender, has been studied before and does not result in low neutron energies that we would like. As result, we are able to conclude that the best source for our purposes will be ^{207}Bi.

2.4 Improved Neutron Rates

The calculations done above for the neutron rates were naive in a few ways. First, we assumed that we would have 1g of gamma source material, when it would be more proper to use the the quoted strength of the gamma sources instead. The target was approximated as a sphere, when it will actually be a cylinder. In addition, the target was assumed to be homogeneous and the mass was severely underestimated. In order to correct for this, we improve upon the calculations below.

The easiest issue to correct is that of the amount of gamma source material. The strengths quoted in Table 1, when multiplied by a scaling factor of 3.7E5, will replace A in Equation 5. Next, the actual target that will be used is BeO, which given a density of $3.02 g/cm^3$ and the dimensions in Figure 4b, yields a target mass of 29.15g. An additional factor of $9/25$ will be picked up in Equation 5 due to the inhomogeneity of the target.

A better estimation of the neutron rate can be found from taking the average value of the distance that an emitted neutron would travel before interacting with the BeO target.

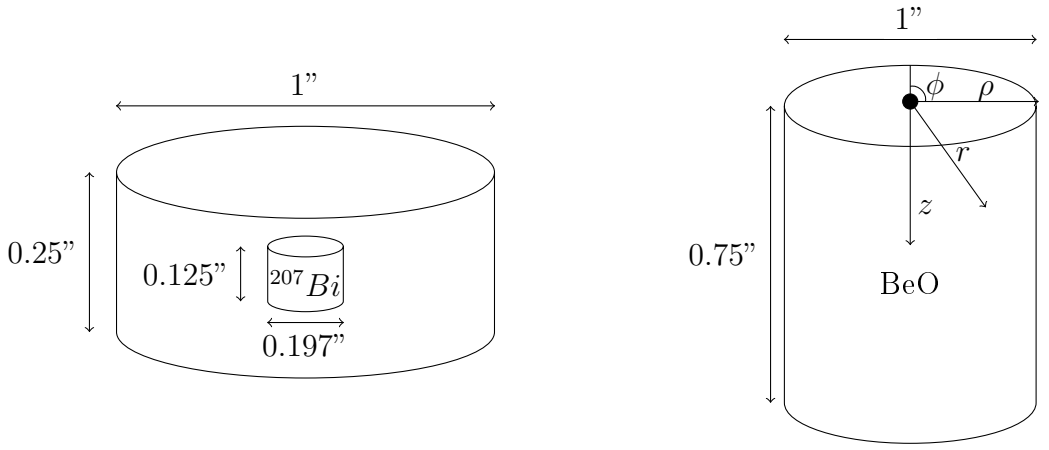

Figure 4: (a) Dimensional drawing of the ^{207}Bi source. The source consists of an active volume located inside a non-active disk. (b) Dimensional drawing of the gamma target, BeO. Integrating over this volume allows for more accurate calculations.

$$\bar{f} = \frac{1}{V} \iiint_D f(\rho, \phi, z) dV \tag{6}$$

Equation 6 shows the generalized formula for averaging a function over a volume V and within a domain D. Applying this equation to our function for estimating the neutron emission rate in Equation 5 yields:

$$\#n \approx A * \%Branching * (\frac{m_{target}}{m_{Be}} * \frac{9}{25}) * \sigma * \frac{1}{V} \int_0^{1.905} \int_0^{2\pi} \int_0^{1.27} \frac{\rho}{4 * \pi * r^2} d\rho d\phi dz \tag{7}$$

$\rho = \sqrt{(r^2 + z^2)}$ is obtained from the coordinate system described in Figure 4b, V is the volume of the BeO cylinder in Figure 4b, and the additional mass factor for an in-homogeneous target has been included. As a sanity check, we can compare our calculated rates with other results. For 1 Ci of ^{88}Y, the expected value is 10E4 N/s/Ci[5]. For 0.1 mCi, we would expect a rate on the order of 10 n/s, and our calculations yield 25.89 n/s. For ^{207}Bi, we now obtain a more accurate neutron emission rate of 0.30 n/s. Having determined a proper gamma source and calculated the expected neutron energy and emission rates, we can now use simulations of our source and chamber to obtain a deeper insight as to how the source will interact and what we can obtain from it.

3 Analysis

GEANT4 is a simulation software that allows for the tracking of particles as they pass through matter, recording properties of each event such as the volume collided with, energies of the particle, scattering types, and more. GEANT4 is highly versatile in its ability to simulate particle events for a wide array of purposes ranging from astroparticle physics to accelerator physics. The software allows for highly detailed and specialized construction of detectors, enabling for high accuracy simulations of many different scenarios.

The first model of the Drexel Bubble Chamber is simulated using the most simplistic version of the detector. The chamber is contained within a box of air, and the chamber is composed of the acrylic container, mineral oil, quartz jar, and C3F$_8$ target. The idea of a particle guide to minimize neutron attenuation when the source is placed outside the mineral oil is also proposed and discussed in a later section. This introduces an additional component to the detector, seen below in Figure 5b. The final version of the chamber includes components from the top of the detector to simulate sources along the z-axis.

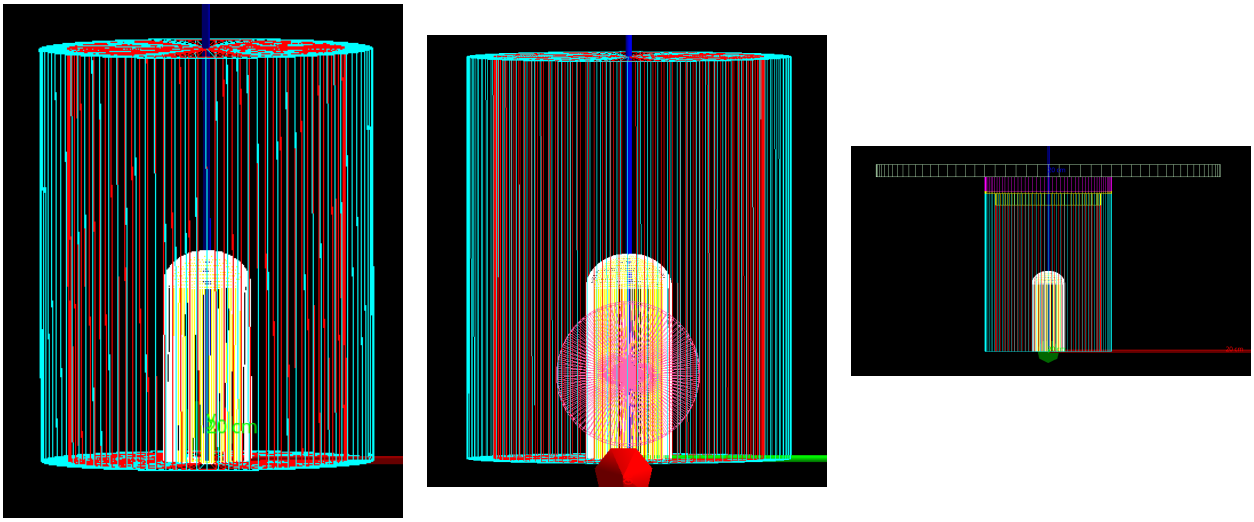

Figure 5: (a) GEANT4 assembly of the relevant Drexel Bubble Chamber volume. The components are colored as: acrylic: cyan, mineral oil: red, quartz: white, C_3F_8: yellow. The surrounding volume is composed of air. (b) The pink material is the inclusion of a particle guide to aid in the neutrons traversing the mineral oil. (c) New design with the addition of the heat bath, plastic insulation, and copper heating plate.

3.1 Emission Type

As seen below in Figure 6, the first thing to consider with our source is how it will emit particles. The ideal situation would be to focus the neutrons to be emitted linearly towards our target volume. Other considered emission types are an arc covering the surface area of the detector and isotropic emission. A linear beam will produce an average energy almost three times stronger than isotropic source, leading to a bubble rate nearly six times larger. In order to focus the neutrons to an arc or linear beam, you would need a material capable of reflecting neutrons without significantly decreasing their energy. There is also no guarantee that the neutrons will be reflected outwards instead of continually scattering inside the shielding. In addition, the source will take up much more volume due to this additional material, making it much less flexible and inconvenient. As a result, we can conclude that it is best to leave the source as an isotropic emitter despite the fact that it is much weaker.

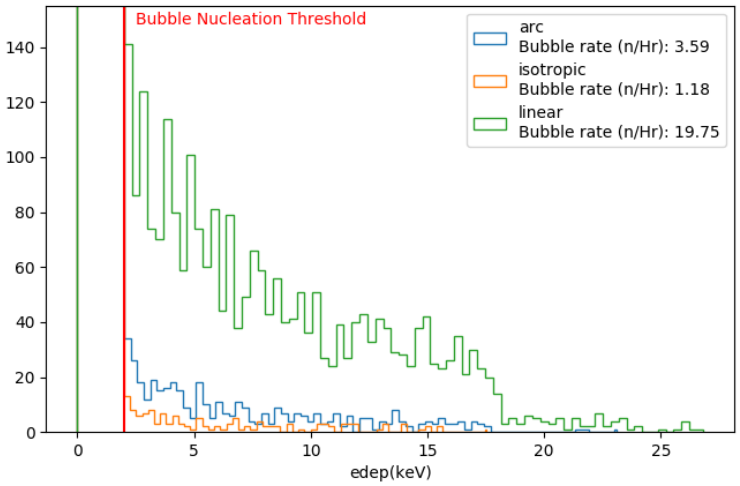

Figure 6: GEANT4 simulation of a neutron source placed 60mm away from the detector. As expected, linear emission performs best, follow by arc and isotropic emissions.

3.2 Distance From Detector

Next, we test for expected rates at varying distances from the chamber: 100mm, 60mm, and 18mm. These three key locations that the neutron source can be placed at correspond to: far away from the chamber, up against the acrylic, or up against the C_3F_8. The results of the simulations can be seen below in Figure 7. Mineral oil strongly attenuates neutrons, greatly reducing both the energies and counts of neutrons that reach the target volume. Hydrogen and other low atomic number elements have high scattering cross sections with neutrons, reducing the likelihood of a neutron passing through unobstructed. Since the mineral oil contains a significant enough composition of Hydrogen, any amount will greatly impact the number of events we expect to see. The source should then be ideally placed within the mineral oil, as close to the quartz jar as possible to minimize the volume of mineral oil that each neutron will have to traverse before detection.

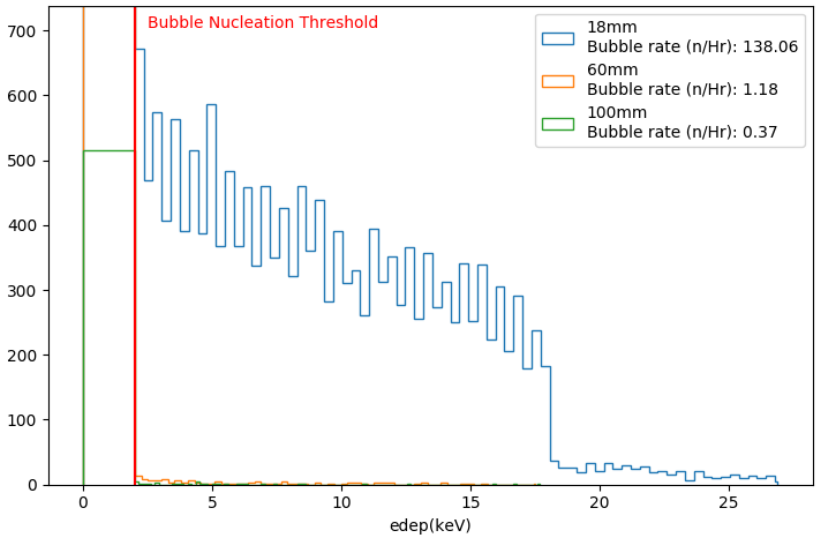

Figure 7: GEANT4 simulations overplotted to show the number of events in the target volume and the average energy of those events. At 100mm, the source was placed far from the detector; at 58mm, the source was placed right outside the mineral oil; and at 16mm, the source was placed inside the mineral, right up against the C_3F_8.

3.3 Particle Guide

Inserting and removing the source from the mineral is a tedious task with a small chamber like the DBC, so it will be exponentially more difficult for the large chambers. An easier method might be to place a particle guide inside the mineral oil that will allow the neutrons to safely traverse through to the C_3F_8 volume. We test with three different materials of air for its low density, copper, and lead, both for their high atomic numbers. The idea here is to displace the mineral oil volume with a higher atomic number or lower density material such that the emitted neutrons would not be attenuated. Looking at Figure 8, we see, as expected, that air performs the best at allowing neutrons to travel through it, follow by lead and then copper. Even in the best case scenario, a particle guide performs significantly worse than placing the source inside the mineral oil.

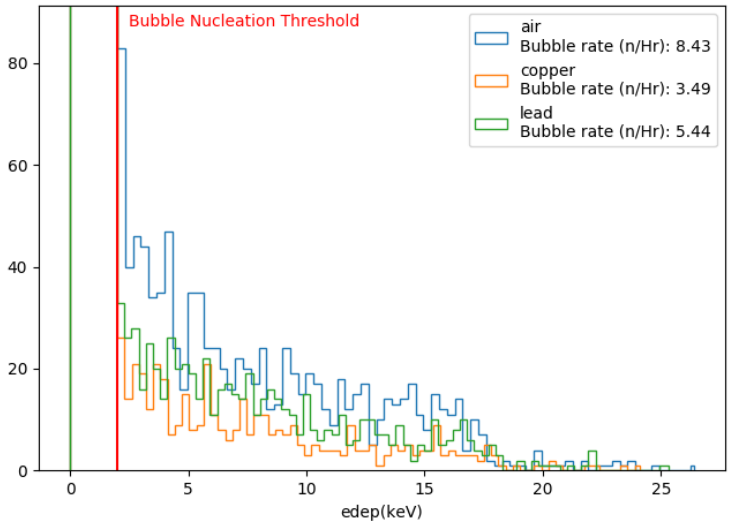

Figure 8: GEANT4 simulations overplotted to show the number of events in the target volume and the average energy of those events. These simulations were run with a particle guide made of air, lead, and copper introduced inside the mineral oil volume.

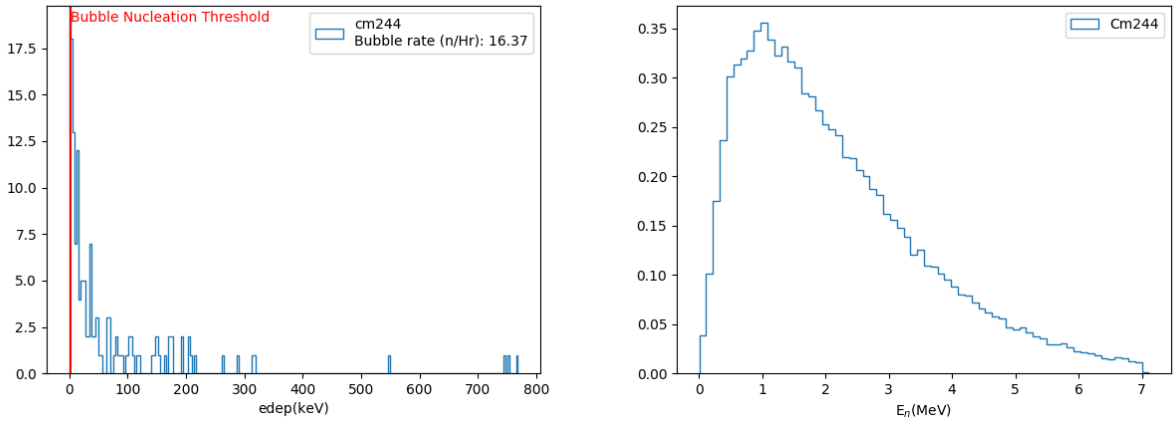

Figure 9: (a) Neutron energy counts when interacting with the target volume. (b) Emission energy spectrum of ^{244}Cm from GEANT4.

3.4 ^{244}Cm Source

We would like to have some indication that the simulations reflect reality before blindly trusting them as indicating any useful results. Experimental data has been previously obtained for a ^{244}Cm source placed directly above the chamber. This source primarily undergoes α decay with a small branching ratio for spontaneous fission. Since this source placed on top of the chamber, it is necessary to include the top components, as mentioned in the discussion on detector construction. From this data, a result of approximately 108 bubbles per hour was obtained. The current activity of the source has been calculated to be 4.64 neutrons/sec.

Using the calculate neutron emission rate, we can simulate the ^{244}Cm source with our chamber and attempt to see if the results match. As seen above in Figure 9b, the emission spectrum of the source is properly replicated; however, the bubble rate shown in Figure 9a is significantly less than our experimental value. This can potentially be explained by (α, n) reactions in the chamber components due to ^{244}Cm undergoing α decay a significant portion of the time. The physics that is being used with the simulation is not capable of detecting an (α, n) reaction, and as a result, the simulation will miss any neutrons produced through that process.

3.5 Bubble Rates

Neutrons within the chamber are usually detected through their bubble multiplicity. With a neutron source, we would then expect to see multiple bubbles per event. By running 100 simulations each with 100,000 events, we simulate our source over a range of threshold energies. Figure 10 shows the the average bubble multiplicity for each energy threshold from the simulations. As a result of the low neutron energies, we should expect to see bubble multiplicity very close to 1. As the threshold increases, the likelihood that a bubble is nucleated decreases, meaning that the bubble multiplicity should also decrease. The average bubble multiplicity can then be used to normalize calculations to a per-event basis rather than counting all bubbles. The 60mm data also shows that there is high error in the results compared to 18mm, so placing the source at 60mm will make it difficult to match experimental results with simulated results. The DBC can be scaled to the approximate sizes of PICO-40 and PICO-500 to see how the source might interact with the large chambers. Due to the increased volume, each threshold has a higher average bubble multiplicity. As seen in Figure 10b, there is a threshold with increasing the volume of the target liquid in

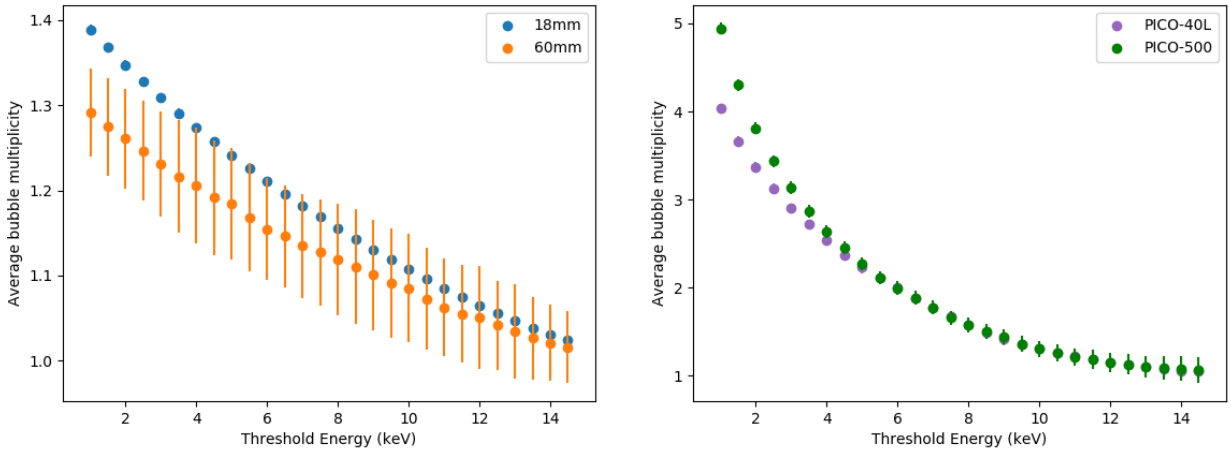

Figure 10: Expected average bubble multiplicities for a range of threshold energies. (a) Source placed 18mm and 60mm from the DBC chamber. (b) DBC chamber scaled to large chambers with source placed within mineral oil.

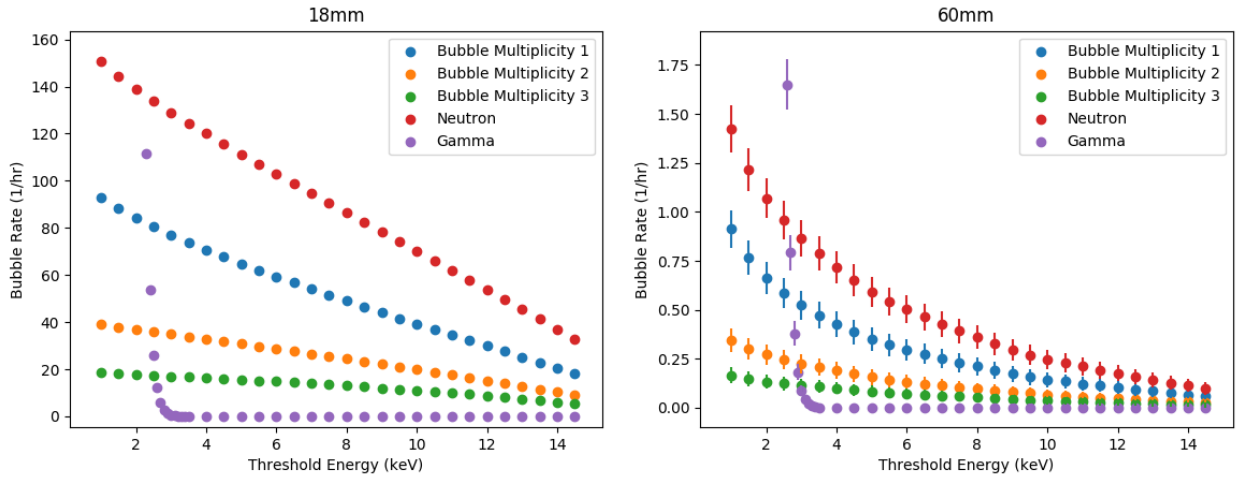

Figure 11: Expected bubble rates as a function of threshold energy at both 60mm and 18mm away from the chamber center. The rates for the neutrons are also broken down in to rates for bubble multiplicities, whose sum is equal to the total neutron rate.

which the bubble multiplicity no longer increases. At this point, the limiting factor becomes the energy of the neutrons rather than the space for more bubbles to nucleate.

The expected bubble rate at a given threshold energy will not only give us an idea of how many events we should expect for a given threshold, but it will also be able to give us an idea of what threshold is being operated at if we know the event rate. We expect the bubble rates to decrease as the threshold energy for nucleation is increased due to less neutrons with sufficient energy coming in contact with the target volume. This effect is observed above in Figure 11 for gammas and neutrons emitted at 18mm and 60mm. It is also important to note that around 2 keV, the gammas emitted from the ^{207}Bi source will dominate the neutrons emitted, making it impossible to differentiate between the two events at lower thresholds when gammas become relevant for bubble nucleation.

Figure 11 also breaks down the composition of the neutron bubbles rates by bubble multiplicity. As expected, lower bubble multiplicities have higher rates than higher multiplicities. For a source placed 60mm away, the error bars show that we would have difficulty differentiating between nearby threshold energies due to significant overlap. This effect is minimized when placed 18mm away due to the large increase in the number of events greater than the

threshold energies. The primary goal of the calibrations is to be able to differentiate WIMP events in the low keV range from other particles such as gammas, so if we can decrease the threshold at which gammas dominate, then finding a WIMP event becomes more likely.

4 Conclusion

We have shown that it is possible to construct a neutron source capable of emitting monoenergetic neutrons in the sub-100 keV energy range. An initial list of seven potential isotopes was filtered down to ^{207}Bi by analyzing the half-lives, branching ratios, expected neutron energies, and expected neutron emission rates. These values were then used in simulating the source and the Drexel Bubble Chamber using GEANT4. We analyzed this source over a variety of different scenarios including emission types, location, chamber composition. From these simulations, we have concluded that placing the source inside the mineral oil will obtain the highest event rates and the most consistent energies. The simulations also show that we should expect the source to be useful until 2 keV, at which point the gammas emitted from the ^{207}Bi source will become a significant event trigger. Several results from the simulations follow expected trends, indicating that the conclusions drawn from them have a valid foundation.

Future plans for the experiment consist of purchasing the gamma source and target to construct the neutron source. Once the source is complete, data taking will begin to compare experimental results with the results from the calculations and simulations done here. The simulation setup and analysis code designed here will form the foundation for future simulations done on the Drexel Bubble Chamber for other sources and scenarios. We can obtain more in depth information as the complexity of the simulations and analysis is built upon by future work. If successful, the source will prove extremely useful for calibrating other chambers. Further success will have the source adapted for use on the primary detector located at Snolab. With the improved calibrations, more stringent limits can be set on the WIMP-nucleon cross section and potentially push us one step closer to detecting dark matter.

References

[1] N. Aghanim et al. (Planck Collaboration). 2018. Planck 2018 results. VI. Cosmological parameters. arXiv:1807.06209

[2] J. I. Collar. 2017. Applications of an ^{88}Y/Be photo-neutron calibration source to Dark Matter and Neutrino Experiments. arXiv:1303.2686

[3] G. Giacomelli. 2006. Introduction to the Workshop "30 years of bubble chamber physics". arXiv:0604152

[4] C. Amole et al. (PICO Collaboration). 2017. Dark Matter Search Results from the PICO-60 C_3F_8 Bubble Chamber. arXiv:1702.07666

[5] C. Amole et al. (PICO Collaboration). 2016. Improved dark matter search results from PICO-2L Run 2. arXiv:1601.03729

[6] C. Amole et al. (PICO Collaboration). 2019. Dark Matter Search Results from the Complete Exposure of the PICO-60 C_3F_8 Bubble Chamber. arXiv:1902.04031

[7] Alvaro E. Chavarria. 2012. Calibrating the energy response of bubble chambers to ^{19}F recoils by taking advantage of the elastic scattering resonances. (PICO Internal Document).

[8] C. Amole et al. (PICO Collaboration). 2018. Measurements and models of the efficiency of bubble nucleation by nuclear and electron recoils in superheated liquids. (PICO Internal Document).

[9] A. Robinson. 2015. Photoneutron Source Characterization and Neutron Simulations.

[10] A. Wattenberg. Photo-Neutron Sources. Preliminary Report No. 6. United States: N. p., 1949. Web. doi:10.2172/4448374.

[11] N. Soppera, M. Bossant, E. Dupont, "JANIS 4: An Improved Version of the NEA Java-based Nuclear Data Information System", Nuclear Data Sheets, Volume 120, June 2014, Pages 294-296.

[12] Chen, J., & Savage, M. J. (1999). np$\rightarrow$dγ for big-bang nucleosynthesis. Physical Review C, 60(6) doi:10.1103/PhysRevC.60.065205

Appendix A: γ-neutron Cross Section Plots

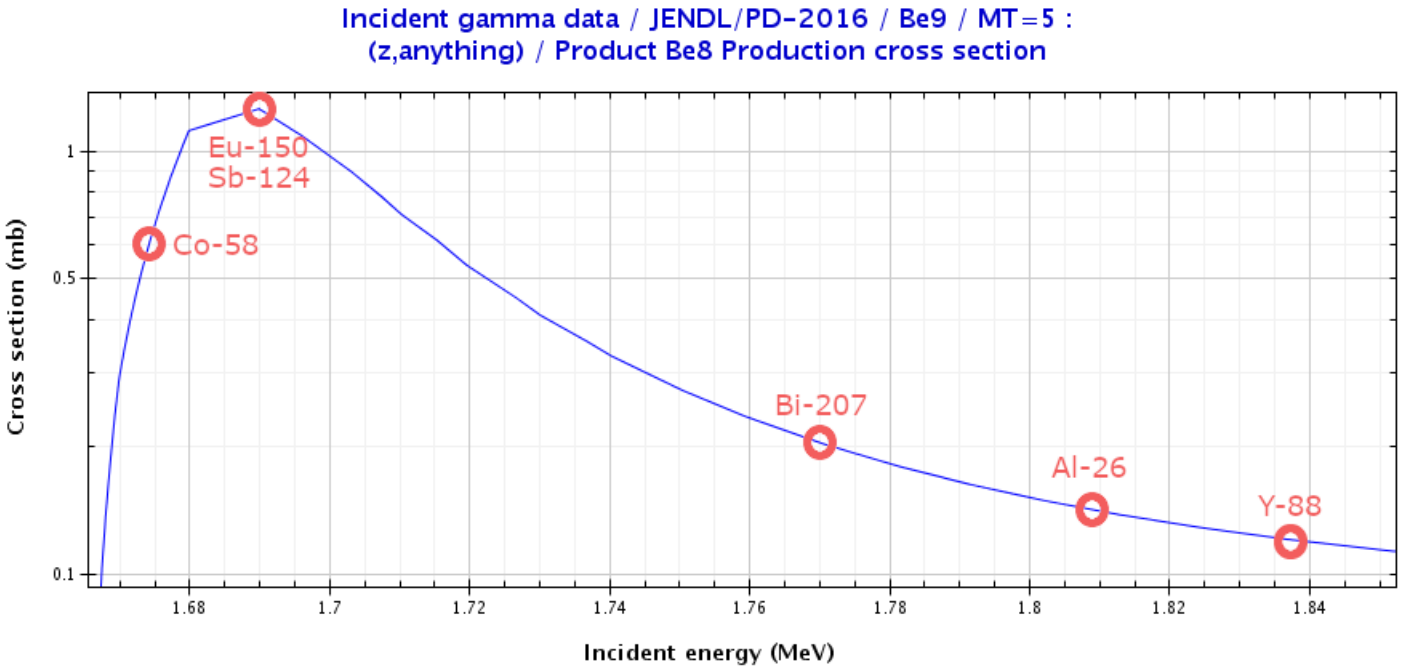

Figure 12: Cross sections for gamma-neutron interactions with a ^{9}Be target as a function of incident gamma energies. Highlighted are the energies of the emitted gammas from each potential source[11].

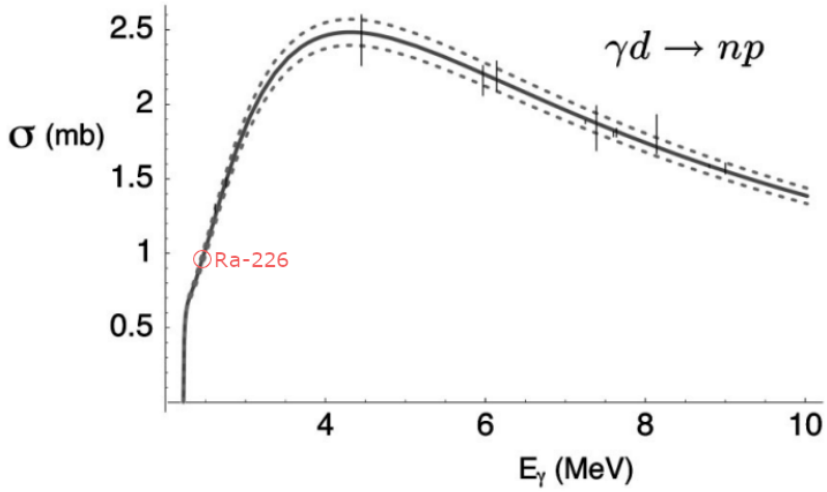

Figure 13: Cross sections for gamma-neutron interactions with a Deuterium target as a function of incident gamma energies. The energy for ^{226}Ra is highlighted[12].